# Translaminar fracture toughness of NCF composites with multiaxial blankets

L.Gigliotti*, S.T. Pinho

*Department of Aeronautics, South Kensington Campus, Imperial College London, SW7 2AZ, London, UK*

**Abstract**

In this paper, the translaminar initiation fracture toughness of a carbon-epoxy Non-Crimp Fabric (NCF) composite laminate was measured using a Compact Tension (CT) test. The translaminar fracture toughness of the individual UD fibre tows was related to that of the NCF laminate and the concept of an homogenised blanket-level translaminar fracture toughness was introduced. Using an approach developed for UD-ply prepreg composites, it is demonstrated that the translaminar fracture toughness of off-axis fibre tows/NCF blankets can be analytically related to that of axially-loaded fibre tows/NCF blankets with a difference between experimentally-measured and predicted values lower than 5%.

*Keywords:* Non-Crimp Fabrics, Translaminar fracture toughness

## 1. Introduction

As a result of the increasing share of composite materials in sectors where cycle times and manufacturing costs significantly impact the final product cost, the development of inexpensive and automated production methods is crucial [1–4].

The need for cost-effective alternatives to conventional prepreg-based composites led to the development of Non-Crimp Fabric (NCF) composites [5–7]. When compared to their prepreg-based counterpart, NCF composites offer higher deposition rates, reduced labour time, higher degree of tailorability and improved impact properties [8–10]. Therefore, NCF composites are widely regarded as one of the most promising technologies for both aerospace [11, 12] and automotive [13, 14] structural composites. The growing industrial interest towards NCF

*Corresponding author. Tel. +44(0)2075945087

*Email addresses:* l.gigliotti12@imperial.ac.uk (L.Gigliotti), silvestre.pinho@imperial.ac.uk (S.T. Pinho)

composites led to two EU-funded research projects: FALCOM [8, 15] and TECABS [16, 17], respectively for aerospace and automotive applications.

Owing to the complex micro-structure of NCF composites, Finite Element (FE) models have been extensively used to investigate their mechanical response at different length-scales [18–21]. Physically-based failure criteria for NCF composites have been proposed by several authors [8, 22]. Nonetheless, these criteria have not yet gained general acceptance due to the extremely high number of input parameters they require, as well as the difficulties in measuring the latter.

Alternatively, state-of-the-art physically-based criteria developed for conventional unidirectional (UD) composites [23–26] can, in principle, be applied to the analysis of NCF composites. However, these criteria do not account for the transverse orthotropy of NCF composites [27]; hence, they require further developments to be capable of accurately predicting relevant failure mechanisms in NCF composites subjected to complex 3D stress states. Molker et al. [28, 29] have proposed a novel set of physically-based failure criteria for NCF composites, based on LaRC05 [30], which account for their transverse orthotropy with an additional failure mode.

Physically-based failure criteria can predict failure at the ply-level and require, as input data, homogenised ply properties which can be measured mostly from standard tests. Particularly, translaminar fracture toughnesses are paramount for the damage-tolerant design of composite structures. Numerous studies have been carried out to characterise the translaminar fracture toughness of UD-ply prepreg composites, e.g. glass/epoxy laminates [31, 32], E-glass fibre-reinforced epoxy laminates [33] and carbon/epoxy laminates [34, 35], as well as of woven composites [36, 37]. However, to the knowledge of the authors, no work has been published on the measurement of the translaminar fracture toughness of NCF composites.

To address this, the translaminar fracture toughness of a carbon-epoxy NCF composite laminate with triaxial ($[45°/0°/-45°]$) blankets is experimentally measured in this work. The translaminar fracture toughness of both the individual UD fibre tows and of the triaxial NCF blanket are determined and the concept of a homogenised NCF blanket-level translaminar fracture toughness was introduced. Furthermore, using an approach developed for UD-ply prepreg composites [38], it is demonstrated that the translaminar fracture toughness of off-axis fibre tows/NCF blankets can be analytically related to that of axially-loaded fibre tows/NCF

blankets.

The present paper is organized as follows: the experimental method and the data reduction scheme for the analysis of experimental results are described, respectively, in Section 2 and Section 3; experimental results are presented and discussed in Section 4. Finally, the main conclusions are drawn in Section 5.

## 2. Experimental method

### *2.1. Material system*

The material used in this work is a triaxial NCF composite produced by Saertex GmbH consisting of Toho Tenax HTS fibres and a polyester knitting yarn, infused with Hexcel RTM6 epoxy resin. The layup of the triaxial NCF blankets, expressed in terms of the UD fibre tows, is $[45°/0°/-45°]$, and their nominal thickness is equal to 0.375 mm (the thickness of the individual fibre tows is 0.125 mm). The nominal membrane properties of the individual fibre tows are listed in Table 1; here, subscripts 1 and 2 denote longitudinal and transverse direction of the fibre tows.

**Table 1:** Nominal membrane properties of the fibre tows in the triaxial NCF blanket [39, 40].

| $E_1$ [GPa] | $E_2$ [GPa] | $G_{12}$ [GPa] | $\nu_{12}$ [−] |
|---|---|---|---|
| 130.00 | 9.00 | 4.50 | 0.26 |

### *2.2. Specimen and layup configuration*

Compact Tension (CT) specimens [41, 42], with dimensions shown in Figure 1 and layups provided in Table 2 were cut using a CNC water-jet cutter. The notches of the specimens were machined using a diamond coated disk-saw to guarantee an accurate and sharp crack tip [43]. In Table 2, each layup is expressed as:

- a *tow-level* layup, defined considering the orientations of the individual UD fibre tows within the triaxial NCF blanket;
- a *blanket-level* layup, defined homogenising the triaxial NCF blankets as UD layers oriented as their 0° fibre tows.

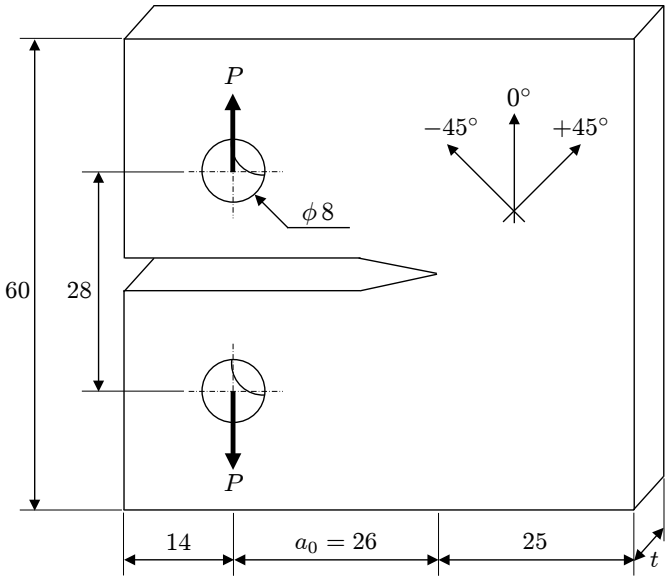



**Figure 1:** CT specimens nominal dimensions (in mm) and fibre directions.

The translaminar fracture toughness of the NCF laminates is denoted as $G_{\mathrm{Ic}}^{A}$ (laminates with layup A) and $G_{\mathrm{Ic}}^{0}$ (laminates with layup B). Furthermore, we define:

- a *tow-level* translaminar fracture toughness (i.e. the translaminar fracture toughness of the individual UD fibre tows within the NCF blankets), denoted as $G_{\mathrm{Ic}}^{0}$ and $G_{\mathrm{Ic}}^{45}$ respectively for the 0° and 45° fibre tows;

- a *blanket-level* translaminar fracture toughness (i.e the translaminar fracture toughness of the entire NCF blankets homogenised as UD layers), denoted as $G_{\mathrm{Ic}}^{\mathrm{NCF}}$.

### *2.3. Test method and experimental setup*

At least five CT specimens were tested for each layup indicated in Table 2 using an Instron machine with a 20 kN load cell; the applied displacement rate was equal to 0.5 mm/min. A video strain gage system was used to measure and record the relative displacement $d$ of two target points drawn on the surface of the specimens (see Figure 2). Load measurements were recorded via the Instron load frame and synchronized with the relative displacement of the two target points measured by the video strain gage system.

**Table 2:** Layups investigated. The nominal thickness of the laminates is indicated as $t^{\text{Lam}}$ and the 0° fibre tows are aligned with the direction of the applied load.

| Layup ID | $t^{\text{Lam}}$ [mm] | Layup | | Purpose of layup |
|---|---|---|---|---|
| | | Tow-level | Blanket-level | |
| A | 6.0 | $[(45°/0°/-45°)_s]_8$ | $[0°]_{16}$ | $G_{\text{Ic}}^{\text{NCF}}$, $G_{\text{Ic}}^{0}$, $G_{\text{Ic}}^{45}$ |
| B | 6.0 | $[(90°/45°/0_2^\circ/-45°/90°)_s]_4$ | $[(45°/-45°)_s]_4$ | $G_{\text{Ic}}^{0}$, $G_{\text{Ic}}^{45}$ |

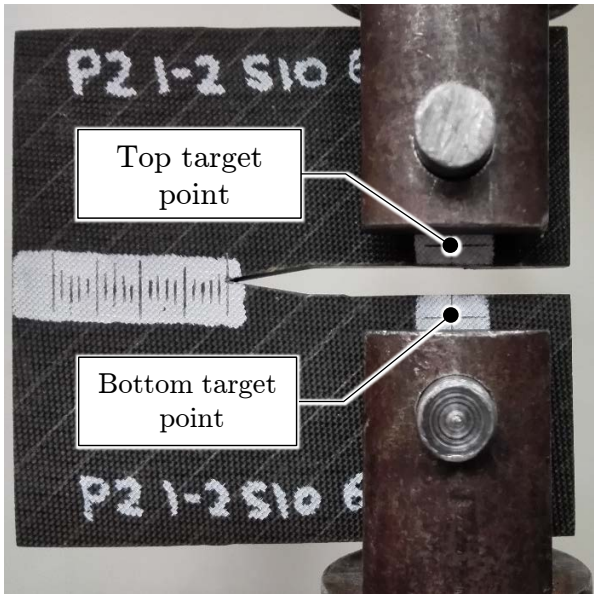



**Figure 2:** Test set up with target points and scale.

## 3. Data reduction

### *3.1. NCF laminate-level translaminar fracture toughness*

The modified compliance calibration (MCC) method [44] was used to calculate the NCF laminate translaminar fracture toughness. Unlike other data reduction schemes, the MCC method does not require optical measurement of the crack length, therefore reducing the operator-dependence of the results. In addition, for the analysis of laminates with different ply orientations, not using the optically measured crack position on the surface is important as the external plies of the specimen often do not reflect the actual crack front within the

specimen during crack propagation, i.e. the crack front is not necessarily uniform across the specimen thickness.

The MCC method requires the elastic compliance $C$ of the CT specimen to be determined at several values of the crack length $a$. For each of the layups in Table 2, an FE model of a half CT specimen (exploiting symmetry) was created in Abaqus [45]. Square 8-noded (S8R5) shell elements with side $l = 0.5\,\text{mm}$ were used. The shape of the initial notch is not explicitly modelled, as the stress intensity factor is not significantly affected by the morphology of the initial opening [46].

A 1 N load was applied at the position of the loading pin. The compliance calibration curve $C$ vs. $a$ was obtained in 0.5 mm increments of the initial crack length (across the whole potential crack growth length). The $C$ vs. $a$ data were fitted with a function of the form [47]

$$C(a) = (\alpha a + \beta)^{\chi}\,, \tag{1}$$

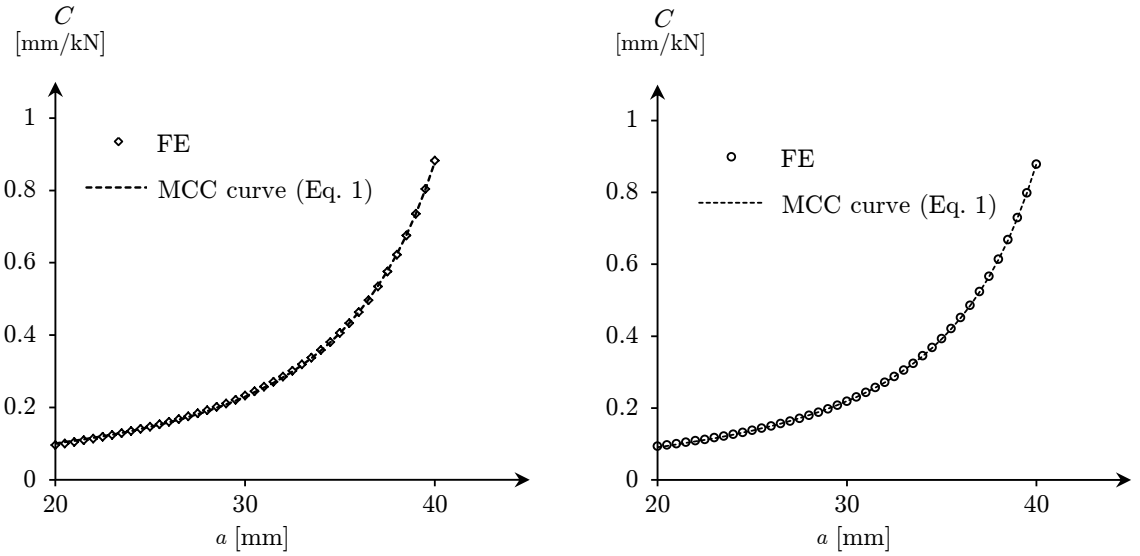
where $\alpha$, $\beta$ and $\chi$ were calculated to best fit the experimental data for each layup; the values of $\alpha$, $\beta$ and $\chi$ for the two layups investigated in this work are provided in Table 3. The compliance calibration curves obtained with FE and the corresponding MCC method fitting curves are shown in Figure 3a (Layup A) and Figure 3b (Layup B).

**Table 3:** Numerical fitting parameters used in the MCC method (units system: kN; mm).

| Layup ID | $\alpha$ | $\beta$ | $\chi$ |
|---|---|---|---|
| A | $-8.944 \times 10^{-2}$ | 4.639 | -2.192 |
| B | $-9.338 \times 10^{-2}$ | 4.796 | -2.205 |

Therefore, an effective crack length $a_{\text{eff}}$ can be determined using the elastic compliance computed from the load vs. displacement curve as

$$a_{\text{eff}} = \frac{C^{\frac{1}{\chi}} - \beta}{\alpha}\,. \tag{2}$$




**(a)** Layup A (see Table 2). **(b)** Layup B (see Table 2).

**Figure 3:** Compliance calibration curves obtained from FE and the MCC method.

Finally, the translaminar fracture toughness of each layup can be calculated as

$$G_{\mathrm{Ic}}^{\mathrm{Lam}} = \frac{P_{\mathrm{c}}^2}{2t}\frac{\mathrm{d}C}{\mathrm{d}a}\,, \tag{3}$$

where $P_{\mathrm{c}}$ is the measured load that propagates the crack.

### *3.2. Fibre tow-level translaminar fracture toughness*

#### *3.2.1. Relating the toughness of the individual fibre tows to the toughness of the laminate*

The fracture toughness of the individual UD fibre tows can be obtained from that of the NCF laminate using a rule of mixture [42, 48]. Thus, the translaminar fracture toughness of the layups investigated in this work, and respectively denoted as $G_{\mathrm{Ic}}^{\mathrm{A}}$ and $G_{\mathrm{Ic}}^{\mathrm{B}}$, can be expressed as

$$G_{\mathrm{Ic}}^{\mathrm{A}} = \frac{t_{\mathrm{A}}^{0}}{t_{\mathrm{A}}}G_{\mathrm{Ic}}^{0} + \frac{t_{\mathrm{A}}^{45}}{t_{\mathrm{A}}}G_{\mathrm{Ic}}^{45} \quad \text{and} \tag{4}$$

$$G_{\mathrm{Ic}}^{\mathrm{B}} = \frac{t_{\mathrm{B}}^{0}}{t_{\mathrm{B}}}G_{\mathrm{Ic}}^{0} + \frac{t_{\mathrm{B}}^{45}}{t_{\mathrm{B}}}G_{\mathrm{Ic}}^{45} + \frac{t_{\mathrm{B}}^{90}}{t_{\mathrm{B}}}G_{\mathrm{Ic}}^{90}\,. \tag{5}$$

where:

- $G_{\mathrm{Ic}}^{0}$, $G_{\mathrm{Ic}}^{45}$ and $G_{\mathrm{Ic}}^{90}$ are, respectively, the translaminar fracture toughness of the 0°, 45° and 90° fibre tows;
- $t_{\mathrm{A}}$ and $t_{\mathrm{B}}$ are, respectively, the thicknesses of specimens with layup A and layup B;
- $t_{\mathrm{K}}^{0}$, $t_{\mathrm{K}}^{45}$ and $t_{\mathrm{K}}^{90}$ are, respectively, the total thicknesses of the 0°, 45° and 90° fibre tows within specimens with generic layup K.

Therefore, assuming that the intralaminar fracture toughness $G_{\mathrm{Ic}}^{90}$ is negligible when compared to the translaminar fracture toughness of the 0° and 45° fibre tows ($G_{\mathrm{Ic}}^{90} << G_{\mathrm{Ic}}^{0}, G_{\mathrm{Ic}}^{45}$) [42], $G_{\mathrm{Ic}}^{0}$ and $G_{\mathrm{Ic}}^{45}$ can be obtained, respectively, as

$$G_{\mathrm{Ic}}^{0} = \left[\frac{t_{\mathrm{A}} t_{\mathrm{B}}^{45}}{t_{\mathrm{A}}^{0} t_{\mathrm{B}}^{45} - t_{\mathrm{A}}^{45} t_{\mathrm{B}}^{0}}\right] \cdot G_{\mathrm{Ic}}^{\mathrm{A}} - \left[\frac{t_{\mathrm{A}}^{45} t_{\mathrm{B}}}{t_{\mathrm{A}}^{0} t_{\mathrm{B}}^{45} - t_{\mathrm{A}}^{45} t_{\mathrm{B}}^{0}}\right] \cdot G_{\mathrm{Ic}}^{\mathrm{B}}\,, \tag{6}$$

$$G_{\mathrm{Ic}}^{45} = \left[\frac{t_{\mathrm{A}}^{0} t_{\mathrm{B}}}{t_{\mathrm{A}}^{0} t_{\mathrm{B}}^{45} - t_{\mathrm{A}}^{45} t_{\mathrm{B}}^{0}}\right] \cdot G_{\mathrm{Ic}}^{\mathrm{B}} - \left[\frac{t_{\mathrm{A}} t_{\mathrm{B}}^{0}}{t_{\mathrm{A}}^{0} t_{\mathrm{B}}^{45} - t_{\mathrm{A}}^{45} t_{\mathrm{B}}^{0}}\right] \cdot G_{\mathrm{Ic}}^{\mathrm{A}}\,. \tag{7}$$

*3.2.2. Relating the toughness of the off-axis fibre tows to that of the* **0**° *and* **90**° *fibre tows*

Teixeira [38] investigated the crack propagation across off-axis plies in prepreg-based CFRPs and showed that a crack propagates across 45° plies through a combination of tensile fibre failure (as in 0° plies under translaminar tension (dashed blue curves Figure 4)) and splits in between fibres (as in 90° plies under intralaminar tension (dashed red curves in Figure 4)). Thus, the translaminar fracture toughness of off-axis plies can, in principle, be expressed as a function of the 0° plies translaminar fracture toughness and of the 90° plies intralaminar toughness.

Therefore, from geometrical considerations, the translaminar fracture toughness of off-axis plies (at an angle $\alpha$ with respect to the 0° fibre tows), denoted as $G_{\mathrm{Ic}}^{\alpha}$, can be estimated as [38]

$$G_{\mathrm{Ic}}^{\alpha} = \cos(\alpha) \cdot G_{\mathrm{Ic}}^{0} + \sin(\alpha) \cdot G_{\mathrm{Ic}}^{90}\,. \tag{8}$$

In the present work, we use the same relation for off-axis fibre tows in an NCF architecture. Therefore, rearranging Equation 8 and neglecting $G_{\mathrm{Ic}}^{90}$, the translaminar fracture toughness of the 0° plies can be independently calculated from the translaminar fracture toughnesses of layups A and B, i.e.

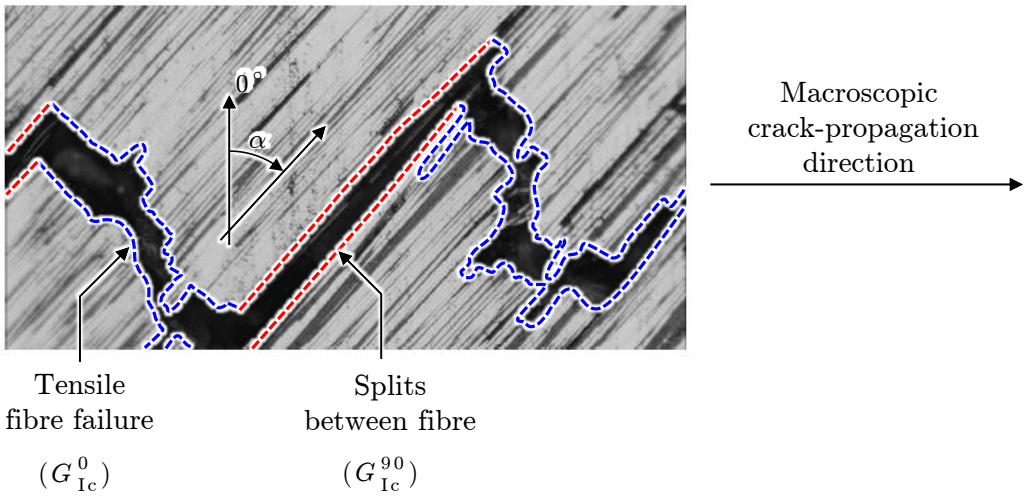



**Figure 4:** Micrograph of a crack propagating across off-axis plies (angle $\alpha$) in a prepreg-based composite laminate, after [38].

$$G_{\mathrm{Ic}}^{0} = \left[ \frac{t_{\mathrm{K}}}{t_{\mathrm{K}}^{0} + \frac{\sqrt{2}}{2} \cdot t_{\mathrm{K}}^{45}} \right] \cdot G_{\mathrm{Ic}}^{\mathrm{K}} \,, \qquad \mathrm{K} \in \{\mathrm{A,B}\} \,. \tag{9}$$

### *3.3. NCF blanket-level translaminar fracture toughness*

Finite Element models of NCF composite laminates are often created by modelling the multi-axial NCF blankets as a single layer of material with homogenised properties. Therefore, physically-based failure criteria as those reviewed in Section 1 require, in addition to the translaminar fracture toughness of the individual UD fibre tows, also the NCF blanket-level translaminar fracture toughness.

The translaminar fracture toughness of the triaxial NCF blanket investigated in this work can be directly evaluated from the measured translaminar fracture toughness of layup A, i.e.

$$G_{\mathrm{Ic}}^{\mathrm{NCF}} = G_{\mathrm{Ic}}^{\mathrm{A}} \tag{10}$$

or, following the approach detailed in Section 3.2.2, from the measured translaminar fracture toughness of layup B, i.e.

$$G_{\mathrm{Ic}}^{\mathrm{NCF}} = \sqrt{2} \cdot G_{\mathrm{Ic}}^{\mathrm{B}} \,. \tag{11}$$

## 4. Results and discussion

### *4.1. Load displacement curves*

Figure 5 shows the experimental load vs. displacement curves for layup A (Figure 5a) and layup B (Figure 5b). All the CT specimens tested exhibited a stick-slip crack-growth during testing. Initial failure of the CT specimens was taken as the first significant load-drop in the load-displacement curves. Final failure of the CT specimens corresponded to compressive failure near the edge opposite to the load application (last significant load-drop in the load-displacement curves).

### *4.2. Translaminar fracture toughness*

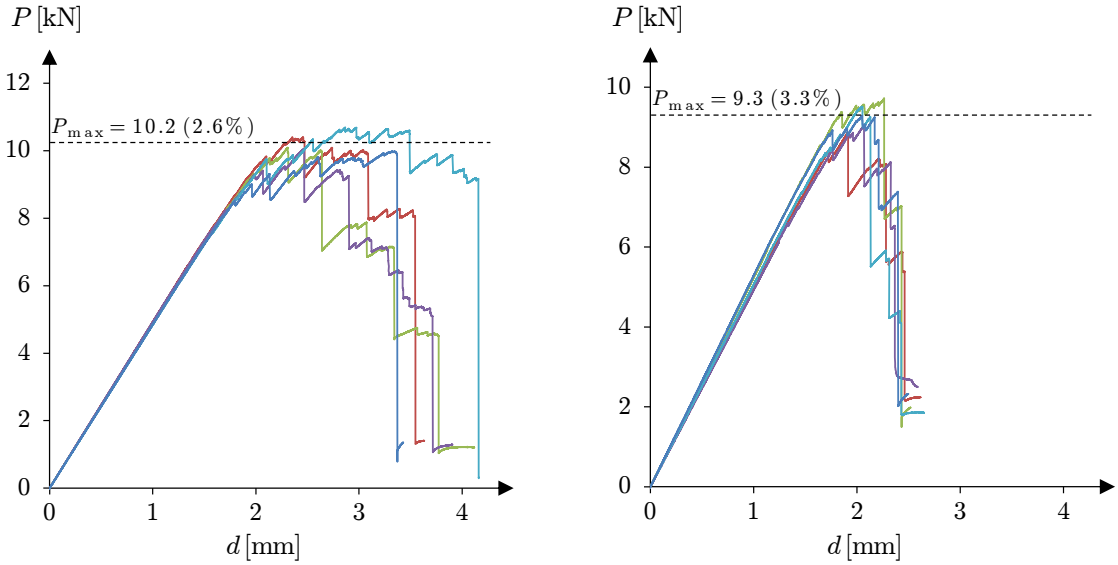
#### *4.2.1. NCF laminate-level translaminar fracture toughness*

Figure 6 shows the R-curves for layup A (Figure 6a) and layup B (Figure 6b). Fracture toughness initiation values are defined as the intersection between the dashed lines at an angle and the vertical axes; although an R-curve effect could be inferred, no meaningful propagation values were obtained as a result of the premature compressive failure of the CT specimens. The average values of the translaminar initiation fracture toughness of layup A and B are provided in Figure 7; the corresponding coefficients of variation are provided in brackets.

#### *4.2.2. Fibre tow-level translaminar fracture toughness*

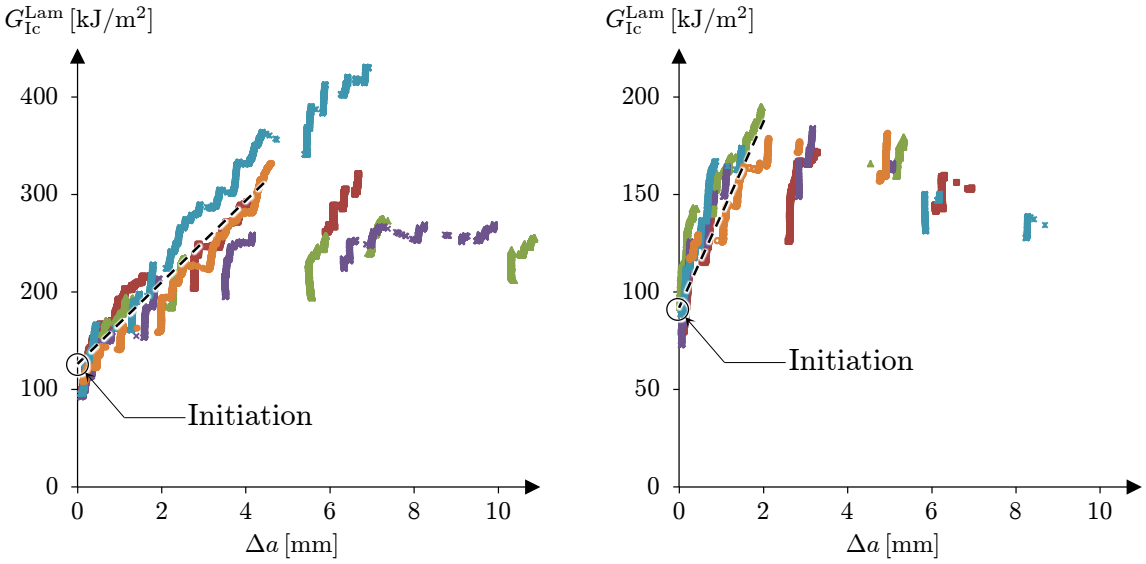
The average values of the translaminar fracture toughness for the UD fibre tows are shown in Figure 8; the corresponding coefficients of variation are provided in brackets. The leftmost and rightmost columns indicate the fracture toughness of the 0° and 45° fibre tows obtained using, respectively, Equations 6 and 7, i.e. from both $G_{\mathrm{Ic}}^{\mathrm{A}}$ and $G_{\mathrm{Ic}}^{\mathrm{B}}$. The second and third columns (from the left) indicate the fracture toughness of the 0° fibre tows predicted independently from $G_{\mathrm{Ic}}^{\mathrm{A}}$ and $G_{\mathrm{Ic}}^{\mathrm{B}}$, using Equation 9.

Quantitatively, the difference between the average value of $G_{\mathrm{Ic}}^{0}$ computed using both $G_{\mathrm{Ic}}^{\mathrm{A}}$ and $G_{\mathrm{Ic}}^{\mathrm{B}}$ (see Equation 6) and that computed exclusively from $G_{\mathrm{Ic}}^{\mathrm{A}}$ is approximately equal to 5 %: furthermore, the difference between the value of $G_{\mathrm{Ic}}^{0}$ computed using both $G_{\mathrm{Ic}}^{\mathrm{A}}$ and $G_{\mathrm{Ic}}^{\mathrm{B}}$ and that computed exclusively from $G_{\mathrm{Ic}}^{\mathrm{B}}$ is approximately equal to 3 %. With regards to the scatter, because Equation 9 uses information from both the 0° fibre tows and the 45°




**(a)** Layup A (see Table 2). **(b)** Layup B (see Table 2).

**Figure 5:** Experimental load ($P$) vs. displacement ($d$) curves for the layups investigated.




**(a)** Layup A (see Table 2). **(b)** Layup B (see Table 2).

**Figure 6:** R-curves for NCF laminate-level translaminar fracture toughness.

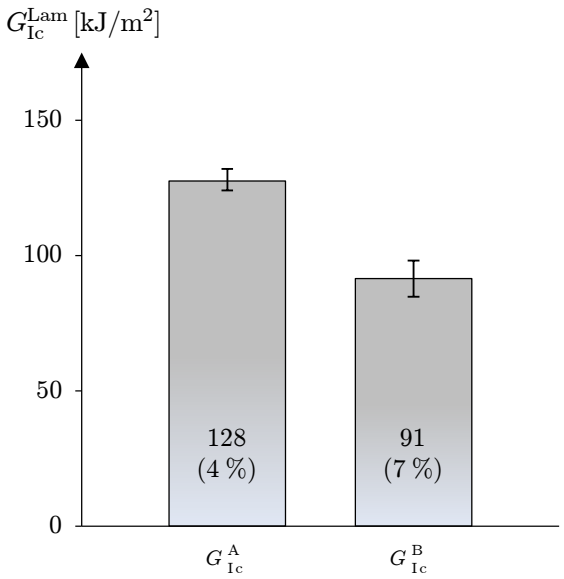



**Figure 7:** NCF laminate-level translaminar fracture toughnesses (initiation values).

fibre tows, while Equation 6 uses only information from the 0° fibre tows, the scatter in the measurements is significantly reduced by using the analytical model expressed in Equation 8.

Therefore, knowing the translaminar fracture toughness of the 0° fibre tows the approach outlined in Section 3.2.2 allows accurate prediction of the translaminar fracture toughness of off-axis fibre tows. Hence, only the translaminar fracture toughness of the 0° fibre tows may be needed to estimate the translaminar fracture toughness of laminates with complex layups (with several differently-oriented off-axis fibre tows). Although further verification is needed for other values of the angle $\alpha$ (see Equation 8), this result is particularly relevant for the design of NCF composite laminates to be used in large-scale structural applications.

*4.2.3. NCF blanket-level translaminar fracture toughness*

Figure 9 shows the average values of the translaminar fracture toughness of the NCF blanket computed according to Equation 10 and Equation 11 (approximate difference of 2 %); the corresponding coefficients of variation are provided in brackets. This result confirms the validity of the approach detailed in Section 3.2.2 also for the prediction of the translaminar fracture toughness of off-axis NCF blankets.

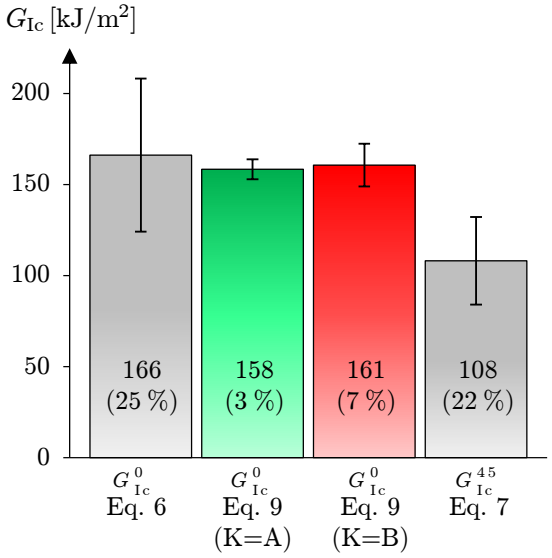



**Figure 8:** Fibre tow-level translaminar fracture toughness (initiation value).

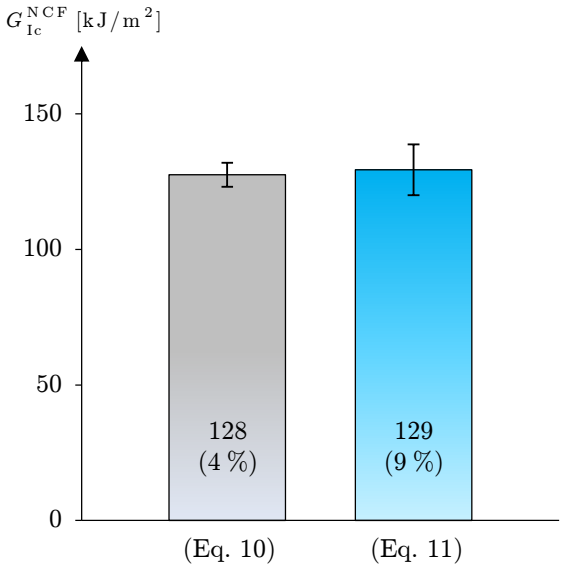



**Figure 9:** NCF blanket-level translaminar fracture toughness (initiation value).

## 5. Conclusions

In this work, the translaminar initiation fracture toughness of a carbon-epoxy NCF composite laminate with triaxial ([45°/0°/−45°]) blankets was measured using a Compact Tension (CT) test; no meaningful propagation values could be determined, as a result of premature compressive failure of the CT specimens. The translaminar fracture toughness of the individual UD fibre tows was related to that of the NCF laminate and the concept of an homogenised blanket-level translaminar fracture toughness was introduced.

In this work, translaminar fracture toughness values were computed neglecting the effect of possible delaminations (inter- and intra-blanket), see Section 3.2.1. Since NCF blankets are stacked such that adjacent fibre tows belonging to different blankets have the same orientation (for both Layup A and Layup B), inter-laminar delaminations are prevented. Moreover, the transverse stitching yarns inhibit the propagation of intra-laminar delaminations.

Using an approach developed for UD-ply prepreg composites [38], it is demonstrated that the translaminar fracture toughness of off-axis fibre tows/NCF blankets can be analytically related to that of axially-loaded fibre tows/NCF blankets. The percentage difference between the values obtained experimentally and those predicted using such analytical approach is, for the material system investigated in this work, lower than 5%. Furthermore, using the analytical model allows to reduce significantly the scatter in the measurements.

Therefore, the translaminar fracture toughness of laminates with complex layups (with several differently-oriented off-axis fibre tows and off-axis NCF blankets) can be accurately estimated from the translaminar fracture toughness of axially-loaded fibre tows/NCF blankets. This result is highly relevant for the design of NCF composite laminates to be used in large-scale structural applications.

## Acknowledgements

The funding from Airbus Operations Ltd (UK) is gratefully acknowledged.

## References

[1] R. Avila-Dominguez, NCF processability and performance - A literature review, Tech Rep. DERA/MSS/MSMA2/WP003564, Farnborough, UK. 2000.

[2] C. Kjelgaard, Challenges in composites, Aircraft Technology 116 (2012) 52–57.

[3] A. Quilter, Composites in aerospace applications, IHS - The Source for Critical Information and Insight, 2010.

[4] G. Marsh, Composites lift off in primary aerostructures, Reinf. Plastics 48 (4) (2004) 22–27.

[5] E. Greenhalgh, Failure analysis and fractography of polymer composites, Elsevier, 2009.

[6] S. Lomov, Non-crimp fabric composites: manufacturing, properties and applications, Elsevier, 2011.

[7] G. Bibo, P. Hogg, R. Backhouse, A. Mills, Carbon-fibre non-crimp fabric laminates for cost-effective damage-tolerant structures, Compos. Sci. Tech. 58 (1) (1998) 129–143.

[8] L. Asp, Local models for NCF composite materials mechanical preformance prediction, in: Proc. 16th Int. Conf. Compos. Mater., 2007.

[9] V. Çeçen, M. Sarikanat, H. Yildiz, I. Tavman, Comparison of mechanical properties of epoxy composites reinforced with stitched glass and carbon fabrics: Characterization of mechanical anisotropy in composites and investigation on the interaction between fiber and epoxy matrix, Polym. Compos. 29 (8) (2008) 840–853.

[10] F. Edgren, L. Asp, P. Bull, Compressive failure of impacted ncf composite sandwich panels-characterisation of the failure process, J. Compos. Mater. 38 (6) (2004) 495–514.

[11] F. Edgren, Physically based engineering models for ncf composites, Ph.D. thesis, KTH (2006).

[12] J. Filsinger, R.-P. Dittmann, T. Bischoff, Textile preforming technologies for fuselage applications, in: Proc. 25th Jubilee Int. SAMPE Eur. Conf. Soc. Adv. Mater. Process Eng., Mater. & Process Tech. - The driver for tomorrow's improved performance, 2004.

[13] BMW formally launches i3 manufacture and assembly, `http://www.compositesworld.com/news/bmw-formally-launches-i3-manufacture-and-assembly` (Sept. 2013).

[14] P. Mårtensson, D. Zenkert, M. Åkermo, Method for the cost-efficient and weight-efficient material diversity and partitioning of a carbon fibre composite body structure, Proc. Inst. Mech. Eng., Part D: J. Autom. Eng., `doi:10.1177/0954407015578037`.

[15] FALCOM, Failure, performance and processing prediction for enhanced design with non-crimp-fabric composites, EU-project, contract No. G4RD-CT-2001-00694.

[16] TECABS, Technologies for carbon fibre modular automotive body structures, Framework

V project G6RD-CT2001-00636, 2000.

[17] I. Verpoest, T. Thanh, S. Lomov, The TECABS Project: Development of Manufacturing, Simulation and Design Technologies for a Carbon Fiber Composite Car, in: Proc. 9th Japan Int. SAMPE Symp., 2005, pp. 56–61.

[18] E. Marklund, L. Asp, R. Olsson, Transverse strength of unidirectional non-crimp fabric composites: Multiscale modelling, Compos. Part B 65 (2014) 47–56.

[19] S. Drapier, M. Wisnom, Finite-element investigation of the compressive strength of non-crimp-fabric-based composites, Compos. Sci. Tech. 59 (8) (1999) 1287–1297.

[20] L. Zhao, N. Warrior, A. Long, Finite element modelling of damage progression in non-crimp fabric reinforced composites, Compos. Sci. Tech. 66 (1) (2006) 36–50.

[21] A. González, E. Graciani, F. París, Prediction of in-plane stiffness properties of non-crimp fabric laminates by means of 3D finite element analysis, Compos. Sci. Tech. 68 (1) (2008) 121–131.

[22] J. Juhasz, R. Rolfes, K. Rohwer, A new strength model for application of a physically based failure criterion to orthogonal 3D fiber reinforced plastics, Compos. Sci. Tech. 61 (13) (2001) 1821–1832.

[23] P. Camanho, C. Dávila, S. Pinho, L. Iannucci, P. Robinson, Prediction of in situ strengths and matrix cracking in composites under transverse tension and in-plane shear, Compos. Part A 37 (2) (2006) 165–176.

[24] S.T. Pinho, C.G. Dávila, P.P. Camanho, L. Iannucci and P. Robinson, Failure models and criteria for FRP under in-plane or three-dimensional stress states including shear non-linearity, NASA/TM-2005-213530, 2005.

[25] S. Pinho, L. Iannucci, P. Robinson, Physically-based failure models and criteria for laminated fibre-reinforced composites with emphasis on fibre kinking: Part I: Development, Compos. Part A 37 (1) (2006) 63–73.

[26] S. Pinho, L. Iannucci, P. Robinson, Physically based failure models and criteria for laminated fibre-reinforced composites with emphasis on fibre kinking. Part II: FE implementation, Compos. Part A 37 (5) (2006) 766–777.

[27] R. Olsson, Experimental observations on the orthotropic transverse strength of Non-Crimp Fabric composites, Tech. Rep. TN15001, Swerea SICOMP, 2015.

[28] H. Molker, D. Wilhelmsson, R. Gutkin, L. Asp, Orthotropic criteria for transverse failure

of non-crimp fabric reinforced composites, Submitted for publication.

[29] H. Molker, R. Gutkin, L. Asp, Implementation of failure criteria for orthotropic non crimp fabric composite structures, in: Proc. 5th ECCOMAS Thematic Conf. Mech. Resp. Compos - COMPOSITES 2015, 2015.

[30] S. Pinho, R. Darvizeh, P. Robinson, C. Schuecker, P. Camanho, Material and structural response of polymer-matrix fibre-reinforced composites, J. Compos. Mater. 46 (19-20) (2012) 2313–2341.

[31] E. Tschegg, K. Humer, H. Weber, Fracture tests in mode i on fibre-reinforced plastics, J. Mater. Sci. 28 (9) (1993) 2471–2480.

[32] K. Humer, E. Tschegg, S. Spiessberger, H. Weber, Fracture mechanical characterization of fibre reinforced plastics in the intralaminar crack opening mode (mode I) and in the shear mode (mode II), Cryogenics 38 (1) (1998) 69–74.

[33] S. Kamiya, H. Sekine, Prediction of the fracture strength of notched continuous fiber-reinforced laminates by interlaminar crack extension analysis, Compos. Sci. Tech. 56 (1) (1996) 11–21.

[34] S. Pinho, P. Robinson, L. Iannucci, Fracture toughness of the tensile and compressive fibre failure modes in laminated composites, Compos. Sci. Tech. 66 (13) (2006) 2069–2079.

[35] G. Catalanotti, P. Camanho, J. Xavier, C. Dávila, A. Marques, Measurement of resistance curves in the longitudinal failure of composites using digital image correlation, Compos. Sci. Tech. 70 (13) (2010) 1986–1993.

[36] J. Masters, Translaminar Fracture Toughness of a Composite Wing Skin Made of Stitched Warp-knit Fabric, NASA/CR-2017283, 1997.

[37] N. Blanco, D. Trias, S. Pinho, P. Robinson, Intralaminar fracture toughness characterisation of woven composite laminates. Part II: Experimental characterisation, Eng. Fract. Mech. 131 (2014) 361–370.

[38] R. Teixeira, Translaminar fracture toughness of CFRP: from the toughness of individual plies to the toughness of the laminate, Ph.D. thesis, Imperial College London (2015).

[39] R. Olsson, Analytical models for impact response and damage growth in sandwich panels, Tech. Rep. CR13-011, Swerea SICOMP, 2013.

[40] T. Block, C. Brauner, M. Zuardy, A. Herrmann, Advanced numerical investigation of

the impact behaviour of CFRP foam core sandwich structures, in: Proc. 3rd ECCOMAS Thematic Confer. Mech. Resp. Compos., 2011.

[41] M. Laffan, S. Pinho, P. Robinson, A. McMillan, Translaminar fracture toughness testing of composites: A review , Polym. Test. 31 (3) (2012) 481–489.

[42] S.T. Pinho, P. Robinson, L. Iannucci, Fracture toughness of the tensile and compressive fibre failure modes in laminated composites, Compos. Sci.Tech. 66 (13) (2006) 2069–2079.

[43] M.J. Laffan, S.T. Pinho, P. Robinson, A.J. McMillan, Translaminar fracture toughness: The critical notch tip radius of 0° plies in CFRP, Compos. Sci.Tech. 72 (1) (2011) 97–102.

[44] M. Laffan, S. Pinho, P. Robinson, L. Iannucci, Measurement of the in situ ply fracture toughness associated with mode I fibre tensile failure in FRP. Part I: Data reduction, Compos. Sci. Tech. 70 (4) (2010) 606–613.

[45] Dassault Systémes Simulia Corp., ABAQUS 6.12 User's Manual, 2012.

[46] W. Jackson, J. Ratcliffe, Measurement of fracture energy for kink-band growth in sandwich specimens, in: Proc. 2nd Int. Conf. Compos. Testing and Model Identification (CompTest 2004), 2004.

[47] C. Dávila, C. Rose, P. Camanho, A procedure for superposing linear cohesive laws to represent multiple damage mechanisms in the fracture of composites, Int. J. Fracture 158 (2) (2009) 211–223.

[48] M. Laffan, S. Pinho, P. Robinson, L. Iannucci, Measurement of the in situ ply fracture toughness associated with mode I fibre tensile failure in FRP. Part II: Size and lay-up effects, Compos. Sci. Tech. 70 (4) (2010) 614–621.